



# Audio Engineering Society Convention Paper

Presented at the 127th Convention  
2009 October 9–12 New York NY, USA

*The papers at this Convention have been selected on the basis of a submitted abstract and extended precis that have been peer reviewed by at least two qualified anonymous reviewers. This convention paper has been reproduced from the author's advance manuscript, without editing, corrections, or consideration by the Review Board. The AES takes no responsibility for the contents. Additional papers may be obtained by sending request and remittance to Audio Engineering Society, 60 East 42<sup>nd</sup> Street, New York, New York 10165-2520, USA; also see [www.aes.org](http://www.aes.org). All rights reserved. Reproduction of this paper, or any portion thereof, is not permitted without direct permission from the Journal of the Audio Engineering Society.*

## A Configurable Microphone Array with Acoustically Transparent Omnidirectional Elements

Jonathan S. Abel<sup>1</sup>, Nicholas J. Bryan<sup>1</sup>, Travis Skare<sup>1</sup>, Miriam Kolar<sup>1</sup>, Patty Huang<sup>1</sup>, Darius Mostowfi<sup>2</sup>, Julius O. Smith III<sup>1</sup>

<sup>1</sup>Center for Computer Research in Music and Acoustics (CCRMA), Stanford Univ., Stanford, CA, 94305, USA

<sup>2</sup>Countryman Associates, Inc., 195 Constitution Drive, Menlo Park, CA, 94025

Correspondence should be addressed to Jonathan S. Abel ([abel@ccrma.stanford.edu](mailto:abel@ccrma.stanford.edu))

### ABSTRACT

An acoustically transparent, configurable microphone array with omnidirectional elements, designed for room acoustics analysis and synthesis, and archaeological acoustics applications, is presented. Omnidirectional microphone elements with 2 mm-diameter capsules and 1 mm-diameter wire mounts produce a nearly acoustically transparent array, and provide a simplified mathematical framework for processing measured signals. The wire mounts are fitted onto a 1.6 cm-diameter tube forming the microphone stand, with the microphones arranged above the tube so that acoustic energy can propagate freely across the array. The wire microphone mounts have some flexibility, and the array may be configured. Detachable arms with small speakers are used to estimate the element positions with an accuracy better than the 2 mm microphone diameter.

### 1. INTRODUCTION

Microphone array technology is widely used, and has found application in specialized fields such as room acoustics analysis and synthesis, and archaeological acoustics [1]. Fig. 1 illustrates an array in use at the Chavín de Huántar archaeological site [1, 2]. For

such applications, a three-dimensional, mechanically robust, and easily maintained system is required. Recent array designs include spherically baffled arrays, unbaffled geodesics, regular polyhedra, and others [3, 4, 5, 6, 7, 8]. While greatly successful, such designs have certain drawbacks. Spherically baffled



Fig. 1: Configurable Microphone Array.

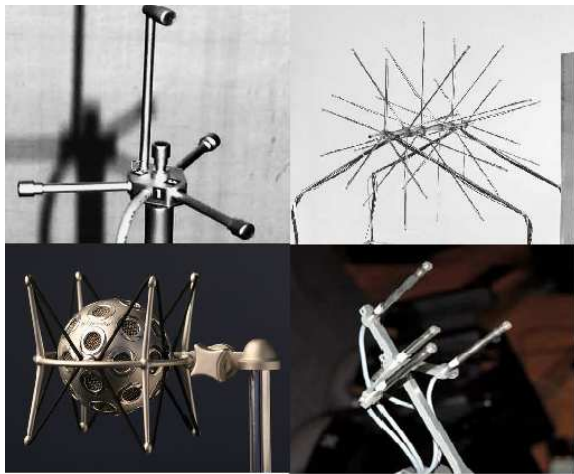


Fig. 2: Example Array Designs [4, 6, 8, 7].

arrays we built suffered from crosstalk between the elements, perhaps due to propagation of mechanical disturbances along the baffle. Such arrays are potentially difficult to transport and maintain in an archaeological acoustics setting where there are limited resources and workspace, and where equipment is exposed to the elements.

The geodesic array described in [4], tetrahedral arrays described in [5, 6, 7] and the like are easier to transport and maintain, but have mounting structures interior to the array, and as a result do not provide an undisturbed acoustic sampling of the soundfield. For an octahedral array design, we found that

sound propagating around its 2 cm-diameter base was attenuated by as much as 0.25dB in the 1.0–5.0kHz range, depending on frequency and arrival direction. Such attenuation, though small, limit the ability to separate sources as a function of direction. What is desired in the context of acoustic analysis and microphone array signal processing (see, e.g., [9, 10]) is a near-perfect sampling of the soundfield, i.e. an array that is *acoustically transparent*.

In this work, we present a microphone array, shown in Figs. 1 and 3, which provides a nearly acoustically transparent sampling of the soundfield at the array elements. The idea is to use small elements and move the microphone base away from the array. In our design, we used sixteen 2 mm-diameter capsule wire mounted omnidirectional microphones. The mounting wires are somewhat flexible and are gathered into a bouquet-like structure, creating a roughly  $16 \times 30 \times 30$  cm size array of microphones attached to a 1.6 cm-wide copper tube, the top of which is about 8 cm below the lowest element of the array. The default configuration occupies a greater extent in the horizontal plane so as to accommodate the relatively greater lateral sensitivity of human hearing needed for our applications.

The acoustically transparent and flexible nature of the design, while advantageous in many regards, requires calibration to determine the microphone positions. Impulse response measurements are used to measure a series of ranges and total direct path energy measurements between known speaker locations and the unknown microphone positions. The range measurements are used to estimate positions, while the direct path energy is used to estimate the relative speaker gains is seen below in §5. A hardware and software calibration system has been developed which produces microphone position estimates having root mean square errors of less than 2.0 mm.

In Section 2, we detail the microphone array design, and in Section 3, its acoustic transparency is evaluated. Section 4 and Section 5 present position and gain calibration methods, Section 6 covers example applications, and Section 7 is a summary.

## 2. ARRAY DESIGN

The proposed microphone array shown in Fig. 3 is a collection of 2 mm-diameter omnidirectional ele-



**Fig. 3:** Configurable Microphone Array.

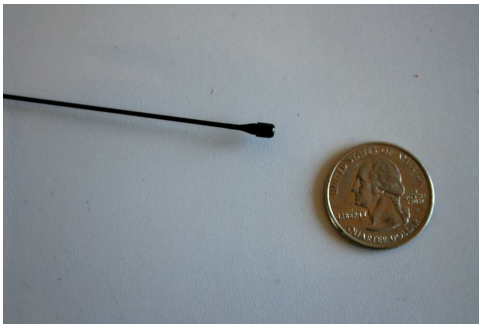


**Fig. 4:** Microphone Element with Mounting Wire

ments (Countryman B6 Omni Lavalier), connected to flexible 1 mm wire mounts. A single microphone element is shown in Fig. 4. The microphone element mounting wires snap onto connectors mounted on a 1.6 cm-diameter copper tube base, which is in turn mounted on a standard camera tripod. Note that the detachable microphone elements, mounting tube, and standard tripod may be compactly stored and are easily transported. Also, microphone elements are easily replaced in the event an element is damaged. Finally, the microphone elements are water-resistant.

To determine the unknown microphone element positions, custom calibration hardware was developed as seen in Fig. 5. The calibration hardware con-

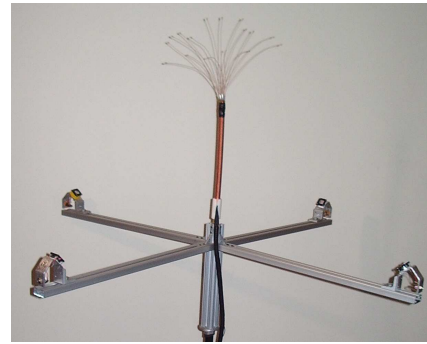


**Fig. 5:** Array with Calibration System.



**Fig. 6:** Calibration Arm

sists of four 2 cm-diameter speakers attached at adjustable, but known locations using 80/20 aluminum bar [11]. A single detached speaker/aluminum bar arm can be seen in Fig. 6. As described in §4, these four speakers are used in sequence to take a series of impulse response measurements for each speaker–microphone pair. Additionally, the calibration hardware was designed to be detachable, leaving the calibrated array ready for any further measurements with a negligible modification to the overall acoustic footprint of the array.

While only three speakers are required for the calibration methods presented, the fourth speaker provides an overdetermined system and is used to improve the accuracy of the resulting position estimator. Additionally, as described in §4.4, it should be noted that the calibration speaker positions were chosen so as to maximize the microphone position estimate accuracy. Before the calibration process and

summary of the results is presented, an evaluation of the acoustic transparency of the array is detailed.

### 3. TRANSPARENCY EVALUATION

To measure the acoustical impact of the microphone mount, we placed the array between an additional reference microphone, also a Countryman B6, and a K&H Model O110 speaker, and measured a series of impulse responses. The reference microphone was placed within the array to act as one of the elements to measure the acoustic contribution of the microphone base as a function of the position of the base relative to the microphone elements. Keeping the speaker and reference microphone at fixed positions, we moved the array vertically over a range of 36 cm, measuring impulse responses every 2 cm. As illustrated in Fig. 7, the first measurement was done with the reference microphone 24 cm above the array base, and the last measurement done with the array base occluding the path between the speaker and reference microphone, 12 cm below the base.

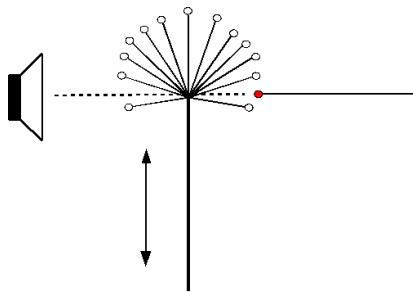


**Fig. 7:** Geometry of Transparency Evaluation.

Transfer function magnitudes were computed for each array position; a reference transfer function magnitude was computed with the array removed. The ratios between the transfer function magnitude and the reference magnitude are plotted as an image in Fig. 8. The measurements show the acoustical impact of placing the microphone mount inside or near the convex hull of the array. Deviation of nearly 1 dB can be seen at close distances, which would result in a significant loss of performance in array processing applications where differences in microphone signal levels are important. Note that with the reference microphone 12 cm or so away from the

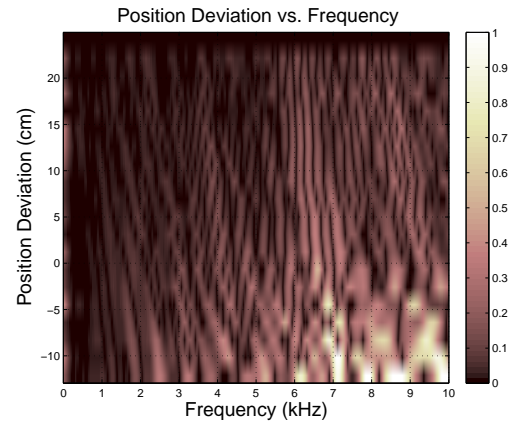


**Fig. 8:** Magnitude Deviation vs. Mount Position; 0 cm corresponds to the tip of the holder being on the speaker-reference microphone axis.

array mount, however, the measured transfer function is within 0.1 dB of the reference value out to 5.0 kHz, as seen in Fig. 3.

### 4. POSITION CALIBRATION

As the array is naturally configurable, it is necessary to determine the microphone element positions. In this section we describe the calibration process with the speaker arms affixed as in Fig. 5.

Impulse response measurements from each speaker-microphone pair are used to determine the speaker-microphone ranges and then the microphone positions. The speaker-microphone range is estimated by cross-correlating the direct path portion of the impulse response with its minimum-phase version [12]. The arrival time is the time of the cross-correlation maximum, and is normalized by the loop-back delay of the measurement system. The arrival time is finally scaled by the speed of sound to give the range between the microphone and speaker.

The microphone locations are then estimated as those minimizing the sum of square range errors to the four speakers. A closed-form divide-and-conquer estimator [13] was used to initialize an iterative Gauss-Newton method for non-linear least squares (GN-NLLS). Speaker-microphone range errors on the order of 2 mm were noted, and micro-

phone position estimate errors less than the 2 mm microphone diameter were seen.

#### 4.1. Time-of-Arrival Estimation

To compute the range, impulse response measurements are computed between each speaker and microphone using a technique similar to that described in [14].

Time-of-arrival estimates  $\tau_{ij}$  between each speaker  $i$  and microphone  $j$  are found by maximizing the correlation between the direct path portion of the impulse response  $h_{ij}(t)$  and its minimum-phase version  $h_{mpij}(t)$

$$\hat{\tau}_{ij} = \operatorname{argmax}_{\tau} \sum_t h_{ij}(t - \tau) h_{mpij}(t). \quad (1)$$

This technique was recently used to estimate interaural time differences [12], and found to be insensitive to the details of the speaker–microphone transfer function magnitude. In this way, the arrival time estimates are expected to be valid even though the speakers generate little energy below 1.0 kHz. It should be pointed out that even though the calibration speakers generate little low-frequency energy, their small size provides a near point source radiation.

#### 4.2. Sound Speed and Loopback Delay

The time-of-arrival estimate must be normalized by the loop-back delay  $\lambda$  of the system and scaled by the speed of sound  $c$  to convert the measured time-of-arrival  $\tilde{\tau}_{ij}$  into a range measurement

$$\tilde{\rho}_{ij} = c(\tilde{\tau}_{ij} - \lambda), \quad (2)$$

where  $\tilde{\rho}_{ij}$  is the measured distance or range in meters between the  $i^{\text{th}}$  microphone and the  $j^{\text{th}}$  speaker. The loopback delay of the system  $\lambda$  can be estimated by simply measuring the closed-loop delay of the system. The sound speed  $c$  is a function of humidity and temperature [15],

$$c = 343.2(1 + 0.0016h) \left[ \frac{T}{T_r} \right]^{\frac{1}{2}}, \quad (3)$$

where  $h$  is the percentage of molar concentration of water vapor,  $T$  is the temperature in degrees Celsius (C), and  $T_r$  is the reference temperature of 293 K.

Commodity humidity and temperature sensors were found to be suitable for such purposes.

To verify the accuracy of the sound speed calculation (2) and the loopback delay measurement, measurements of the time delay  $\tilde{\tau}$  were made at a set of known ranges  $\rho$ . The sound speed and loopback delay were then estimated as the minimizers of the sum of square errors between the measured and hypothesized ranges,

$$\{\hat{c}, \hat{\lambda}\} = \operatorname{argmin}_{c, \lambda} \sum_n (\rho_n - c(\tilde{\tau}_n - \lambda))^2. \quad (4)$$

As seen in Fig. 9, the estimated loopback delay and sound speed accurately reproduce the measured speaker-microphone ranges (the root mean square error was on the order of 2 mm, coincidentally the microphone diameter). Furthermore, the estimated loopback delay and sound speed matched those produced by direct measurement and (3) to within 0.1%.

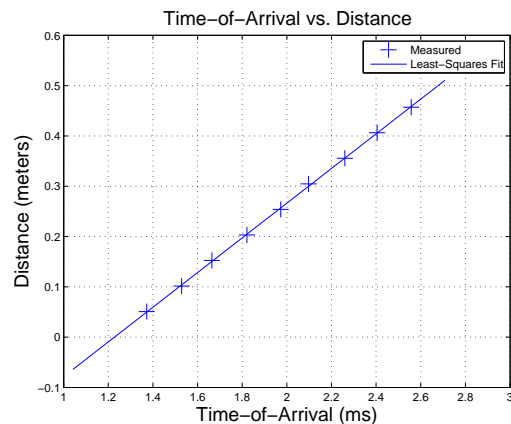


Fig. 9: Sound Speed and Loopback Estimation.

#### 4.3. Microphone Position Estimation

Denote by  $\mathbf{x}_i$ , the  $i$ th microphone position and  $\mathbf{s}_j$ ,  $j$ th the speaker position where  $i = 1, 2, \dots, N$  and  $j = 1, 2, \dots, M$ , with  $N$  and  $M$  the number of microphones and speakers, respectively. For a given set of positions, the hypothesized ranges between each speaker and microphone is

$$\rho_{ij} = \|\mathbf{x}_i - \mathbf{s}_j\|. \quad (5)$$

Given a set of range measurements  $\tilde{\rho}_{ij}$ , the microphone positions are estimated as those minimizing the sum of square differences between the measured and hypothesized ranges,

$$\hat{\mathbf{x}}_i = \underset{\mathbf{x}_i}{\operatorname{argmin}} \sum_j [\tilde{\rho}_{ij} - \rho_{ij}(\mathbf{x}_i)]^2. \quad (6)$$

This was done using a Gauss-Newton iteration [16], initialized with an average of the four three-speaker solutions described in [13]. The position update is

$$\mathbf{x}_i^{(k)} = \mathbf{x}_i^{(k-1)} + (\mathbf{J}^T \mathbf{J})^{-1} \mathbf{J}^T \boldsymbol{\epsilon}^{(k-1)}, \quad (7)$$

where  $\mathbf{J}$  is the Jacobian at iteration  $(k-1)$

$$\mathbf{J} = \begin{bmatrix} \boldsymbol{\beta}_{11}^T \\ \vdots \\ \boldsymbol{\beta}_{1N}^T \end{bmatrix}, \quad (8)$$

where  $\boldsymbol{\beta}_{ij}$  is the column direction cosines between the  $(k-1)$  position estimate  $\mathbf{x}_i^{(k-1)}$  and the  $j^{\text{th}}$  speaker  $\mathbf{s}_j$ ,

$$\boldsymbol{\beta}_{ij} = (\mathbf{x}_i^{(k-1)} - \mathbf{s}_j) / \|\mathbf{x}_i^{(k-1)} - \mathbf{s}_j\|, \quad (9)$$

and where  $\boldsymbol{\epsilon}^{(k-1)}$  is the difference between the measured and hypothesized ranges,

$$\boldsymbol{\epsilon}^{(k-1)} = \begin{bmatrix} \tilde{\rho}_{i1} - \rho_{i1}(\mathbf{x}_i^{(k-1)}) \\ \vdots \\ \tilde{\rho}_{iN} - \rho_{iN}(\mathbf{x}_i^{(k-1)}) \end{bmatrix}. \quad (10)$$

Note that in the presence of Gaussian measured range errors, (6) is the maximum likelihood estimate.

As an example application, the array shown in Fig. 10 was calibrated with the calibration speakers placed at 0.58 m from the array holder center. The estimated microphone positions are shown in Fig. 11 and 12, and appear to closely match the photographed positions. A root mean square range error of slightly less than the 2 mm microphone diameter was noted. Taking into account the speaker geometry, this range error should translate the speaker geometry into a roughly 1.4 mm position error.

#### 4.4. Calibration Geometry Evaluation

The accuracy with which the microphone position estimator is dependent on the geometry of the calibration speaker array. If the speakers are close to the

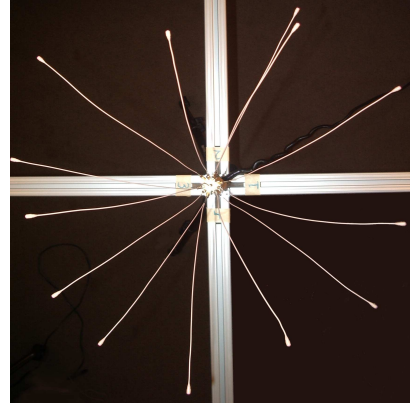


Fig. 10: Image of Top View.

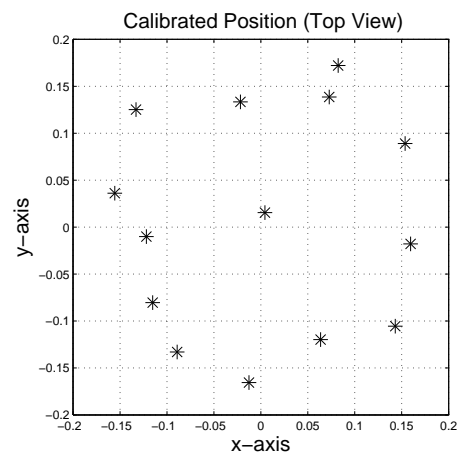
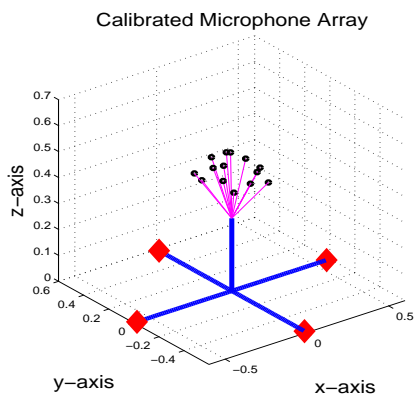


Fig. 11: Computed Top View.

array holder, ranges measured to the microphones will accurately give the vertical positions, but will not have the geometric leverage required to determine the horizontal components of the microphone positions. Similarly, if the speakers are positioned far from the array holder, the microphone signals are weaker, the ranges are less accurately estimated, and the geometry favors estimation of only the horizontal components of the microphone positions.

In this section, we outline a procedure for determining the arm length giving the most accurate microphone position estimates. The approach we take is to evaluate the information inequality [17]—which lower-bounds the estimate variance—over a range of



**Fig. 12:** Calibrated Array.

arm lengths. Because the range measurement errors are a small fraction of the ranges, the position Fisher information is large, and we expect the bound variance to approximate the variance of the position estimator (6).

The needed bound was developed for position estimates based on range measurements in [18], with the bound variance given by the inverse Fisher information  $\mathbf{F}^{-1}$ , interpreted as the outer product of the direction cosines between the microphone and speakers  $\beta_{ij}$ ,

$$\text{Var}\{\hat{\mathbf{x}}_i\} \geq \mathbf{F}^{-1} \quad (11)$$

$$\mathbf{F} = \mathbf{B}^T \Sigma_i^{-1} \mathbf{B} \quad (12)$$

$$\mathbf{B} = [\beta_{i1} \ \dots \ \beta_{iM}] \quad (13)$$

where  $\Sigma_i$  is the range measurement covariance, assumed to be

$$\Sigma_i = \sigma^2 \text{diag} \left\{ \frac{\rho_{ij}^2}{\rho_o^2} \right\}. \quad (14)$$

The range measurement covariance is diagonal, as the ranges are derived from separate impulse response measurements with independent additive noise; they are proportional to the square range due to spherical spreading.

For a measure of the position deviation as a function of calibration geometry, the maximum of the trace of the bound over all microphones is used to evaluate a given speaker geometry.

$$\max_i \text{tr} \{ \mathbf{F}^{-1}(x_i; s) \} \quad (15)$$

An optimal speaker position deviation bound is found by minimizing this trace:

$$s_{opt} = \underset{s}{\text{argmin}} \left\{ \max_i \text{tr} \{ \mathbf{F}^{-1}(x_i; s) \} \right\} \quad (16)$$

Using the example array in Fig. 5, the Fisher information was computed as a function of the x-y speaker position. An optimal speaker position of 0.45 meters was found using (16). The optimal position was verified by adjusting the speaker arm length, re-calibrating the system for the updated speaker positions, and comparing the the average root mean square error between the hypothesized and measured ranges.

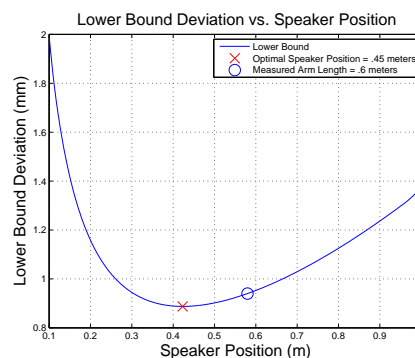


**Fig. 13:** Maximum Position Deviation Bound.

Fig. 13 shows that the lower bound deviation increases as the speaker position approaches the microphone mount or extends beyond the optimal position as expected.

## 5. GAIN CALIBRATION

In addition to the microphone position calibration, it is beneficial to estimate the relative microphone gains of each microphone element. While the relative microphone gains can be easily measured individually using a single fixed speaker–microphone setup, it is possible to obtain a suitable estimate using the set of impulse responses taken for position estimation.

The direct path energy of a given impulse response can be used to estimate the relative gain for each

element. The sum of the square direct path impulse response is used to estimate the direct path energy,

$$e_{ij} = \sum_n h_d^2(n). \quad (17)$$

The relative microphone gains can then be computed as the weighted square root of the direct path energy

$$\hat{g}_{ij} = \alpha(\theta_{ij})\rho_{ij}\sqrt{e_{ij}}, \quad (18)$$

where  $\rho_{ij}$  compensates for spherical spreading loss and  $\alpha(\theta_{ij})$  compensates for the speaker radiation pattern loss as a function of angle between the speaker–look bearing and speaker–microphone bearing as depicted in Fig. 14.

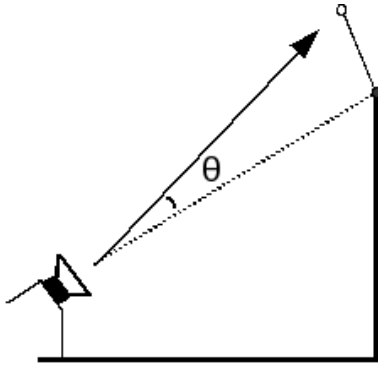


**Fig. 14:** Speaker-Microphone Bearing Angle.

The set of individual microphone gain estimates for each speaker are then normalized by the mean speaker gain over all microphones. The mean microphone gain over the set of speakers is then computed to estimate the relative microphone gains. Note, the median microphone gain over the set of speakers may also be useful to suppress the influence of measurement outliers.

The required  $\alpha(\theta)$  was estimated by a polynomial approximation of the total direct path energy as a function of angle  $[-90^\circ, 90^\circ]$ . Figs. 15 and 16 show the directional response of the speaker and total direct path energy respectively.

Using the example array in Fig. 5 and an eighth-order polynomial approximation of direct path energy, Fig. 17 shows the relative microphone gain estimates and respective standard deviation on the order of 0.25–0.5 dB across the four calibration speakers.

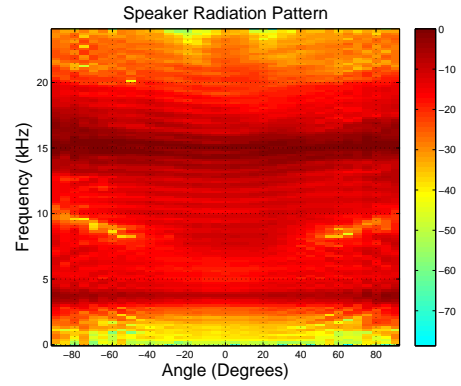


**Fig. 15:** Direct Path Frequency Response.

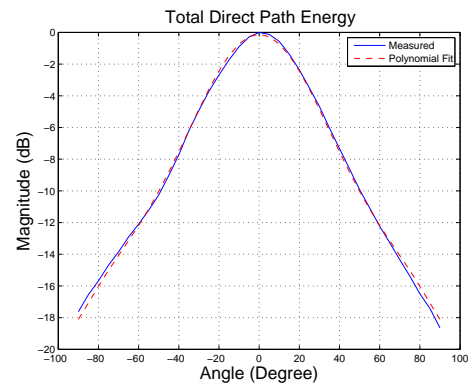


**Fig. 16:** Total Direct Path Energy vs. Angle.

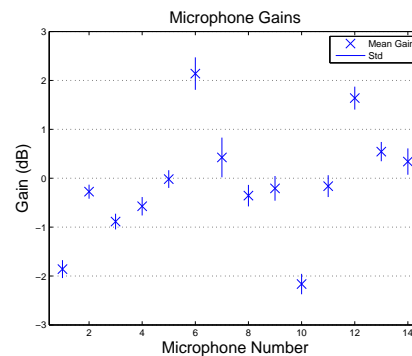


**Fig. 17:** Microphone Element Gain Estimate.

## 6. EXAMPLE PROCESSING

We present two example applications, one where the array was used to track the location of sources, and another where we studied reverberation characteristics of a room through analysis of impulse arrival angles and times. For both experiments, a calibrated array was used for time-delay-of-arrival (TDOA) or direction-of-arrival (DOA) algorithms such as Maximum Likelihood or Multiple Signal Classification (MUSIC) to obtain a plot of signal strength as a function of time and angle of arrival. These algorithms are described briefly below and in more detail in [9, 19].

### 6.1. Maximum Likelihood

Given a calibrated array of  $N$  microphones, the angular direction of a sound source can be computed using a maximum likelihood approach. As the location can be time-varying, the signals are windowed into overlapping frames of 10–100 ms. For microphone  $n$  and frame  $k$ , we have signal  $x_{n,k}(t)$ . Assuming far field sources, we obtain the likelihood dependent on angle  $\theta$  by time-delaying or advancing  $x_{n,k}(t)$  relative to the origin. The adjusted signals,  $x'_n(\cdot)$ , are the original signals as seen from the center of the array, assuming the source is located in the far field at angle  $\theta$ .

We then subtract out the mean signal  $\overline{x'_{n,k}}(t)$  from each of the time-adjusted signals. For correct values of  $\theta$ , the estimated signal will be correct and the difference signals  $x' - \overline{x'}$  will be small. For directions away from the source direction, we are left with a larger error that will be penalized in the likelihood function.

We may maximize the log-likelihood of the error or a similar function thereof; for this specific trial we maximized

$$\mathcal{L}(\theta) = \sum_{i=1}^N \left[ \frac{x_i^T \overline{x}}{(x_i^T x_i * \overline{x^T \overline{x}})^{0.4}} \right]$$

Note that the exponent of 0.4 (rather than the standard 0.5) in the denominator was seen to provide a good visualization of source energy.

We can visualize the likelihood as in Fig. 18 over all  $(\theta, k)$  pairs and plainly see the three known speaker sources located around the array where brighter areas represent high likelihood.

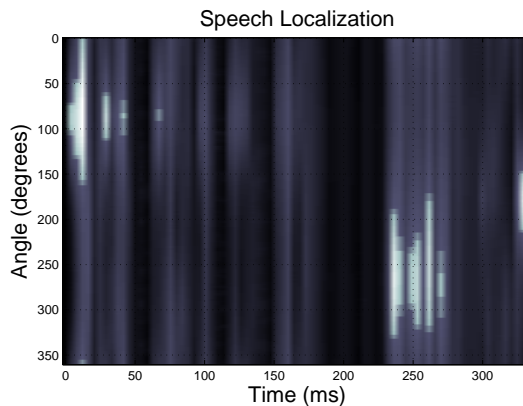


**Fig. 18:** Estimated speech signal strengths as a function of arrival angle and time.

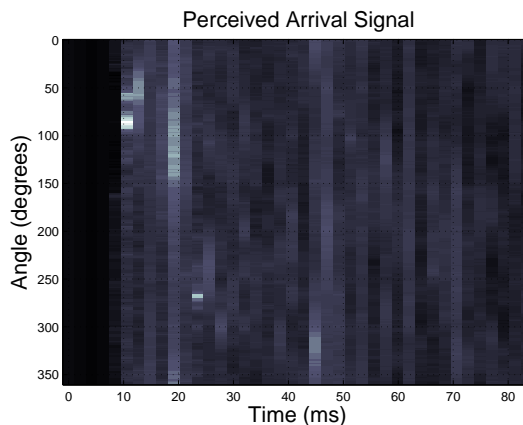


**Fig. 19:** Estimated impulse response strength as a function of arrival angle and time.

### 6.2. MUSIC

Multiple Signal Classification (MUSIC), is an eigenspace-decomposition method that may be used as an alternative to likelihood functions as introduced in [19, 9]. MUSIC operates under the assumption that there are  $M$  far-field signals. Our experiments involve known values of  $M$  or studying perceived plots across several  $M$ , although there are heuristics for finding a likely or optimal value.

The algorithm finds the eigenvectors  $\gamma_n$  of the covariance matrix for our signals in the spectral domain,  $X_n(k)$ . The  $M$  of these corresponding to the largest

eigenvalues will be treated as signal vectors, and the remaining eigenvectors correspond to the (orthogonal) noise subspace.

As described as Broadband MUSIC in [9], we again use a cost function to determine our true direction of arrival  $\theta$ ,

$$\mathcal{L}_{MUSIC}(\theta) = \left[ \sum_{n=M+1}^N \gamma_n^T(\theta) R_a(\theta) \gamma_n(\theta) \right]^{-1},$$

where  $R_a$  is the spectral signal autocorrelation matrix.

As in §6.1, this cost function may be used to generate a plot of arrival energy vs. direction of arrival and time of arrival. Fig. 19 shows the likelihood distribution of an impulse response over time in a reverberant staircase. We see the expected direct-path arrival, followed by early reflections from the wall, and a dense late-field.

## 7. CONCLUSIONS

A new microphone array based on wire-mounted microphones was presented for room acoustics and archaeological acoustics applications. The wire-mounted microphones allow for flexibility in shaping the array, while mitigating the acoustic impact of the array base. However, measurement tasks require a calibration step, as the microphone positions will be different after each setup. To solve this problem, an automated hardware/software calibration system was created that measures time delay of arrival to accurately localize the microphones.

## 8. ACKNOWLEDGEMENTS

We would like to thank D2M for providing us mechanical engineering services and design support, Countryman Associates for donating the microphone elements, and Meyer Sound and Sennheiser Palo Alto Research Center for providing speakers. This work was supported in part by a grant from SiCa, the Stanford Institute for Creativity and the Arts.

## 9. REFERENCES

- [1] J. S. Abel, J. W. Rick, P. Huang, M. A. Kolar, J. O. Smith, J. M. Chowning, "On the

Acoustics of the Underground Galleries of Ancient Chavín de Huántar, Peru," Invited paper Acoustics '08, Paris, France, July 2008.

- [2] M. A. Kolar, J. W. Rick, J. S. Abel, P. Huang, J. O. Smith, J. M. Chowning, P. R. Cook, "Auditory Implications of Gallery Acoustics at Chavín de Huántar," Presentation at Institute of Andean Studies 49th Annual Meeting, Berkeley, CA, 9 January 2009.
- [3] J. Meyer and G. Elko, "Spherical Microphone Arrays for 3D Sound Recording," in *Audio Signal Processing for Next-Generation Multimedia Communication Systems*, Y. (Arden) Huang and J. Benesty, Eds., chapter 2, Kluwer Academic, Boston, Mass, USA, 2004.
- [4] B. N. Gover, J. G. Ryan, M. R. Stinson, "Designing a spherical microphone array for the directional analysis of reflections and reverberation," Convention Paper 5862, Presented at the 115th Audio Engineering Society Convention, New York, October 10–13, 2003.
- [5] Y. Yamasaki and T. Itow, "Measurement of spatial information in sound fields by closely located four point microphone method," *J. Acoust. Soc. Japan(E)*, 10(2), 101110, 1989.
- [6] C. Choi, L. Kim, S. Doo, Y. Oh and K. Sung, "Measurement of Early Reflections in a Room with 5 Microphones System", *IEICE Trans. on Fundamentals of Electronics, Communications and Computer Sciences*, Vol.e 86-A, No. 12, pp. 3283-3287, December, 2003.
- [7] Y. Oikawa, "Spatial Information of Sound Fields," In Havelock, David; Kuwano, Sonoko; Vorlnder, Michael (Eds.), *Handbook of Signal Processing in Acoustics* (p. 1403-1421). New York, Springer 2008.
- [8] em32 Eigenmike microphone array, mh acoustics LLC. <http://www.mhacoustics.com>
- [9] J. Benesty, J. Chen, Y. Huang. "Microphone Array Signal Processing," Springer 2008.
- [10] M. Brandstein, D. Ward (Eds.), "Microphone Arrays: Signal Processing Techniques and Applications," Springer 2001.

- [11] 80/20 Inc., 1701 South 400 East, Columbia City, IN 46725. <http://www.8020.net/>.
- [12] J. Nam, J. S. Abel, and J. O. Smith III, "A Method for Estimating Interaural Time Difference for Binaural Synthesis," Convention Paper 7612. Presented at the 125th Convention, San Francisco, October 25 (2008).
- [13] J. S. Abel, "A divide and conquer approach to least-squares estimation," Aerospace and Electronic Systems, IEEE Transactions on, vol.26, no.2, pp.423-427, Mar 1990.
- [14] Angelo Farina, "Simultaneous measurement of impulse response and distortion with a swept-sine technique," Convention Paper 5093. Presented at the 108 Convention, Paris, February 19-22, 2000.
- [15] ANSI S1.26-1995, American National Standard Method for the Calculation of the Absorption of Sound by the Atmosphere, 2009.
- [16] S. Boyd, "Lecture Notes for EE263," Department of Electrical Engineering, Stanford University, <http://www.stanford.edu/class/ee263/>.
- [17] E. L. Lehmann, "Theory of Point Estimation," John Wiley and Sons 1983.
- [18] J. S. Abel, J. W. Chaffee, "Integrating GPS With Ranging Transponders," Proceedings of the 1991 National Technical Meeting of the Institute of Navigation, Phoenix, AZ 1991.
- [19] R.O. Schmidt. "Multiple Emitter Location and Signal Parameter Estimation," IEEE Trans. Antennas Propagation, Vol. AP-34 (March 1986), pp.276-280.